Heliyon 10 (2024) e32865

Contents lists available at ScienceDirect

Heliyon

journal homepage: www.cell.com/heliyon

Research article

Effect of Mo and W underlayers on ordered phase formation in Fe-Au-Pd multilayer thin films at low temperatures

Szilvia Gulyás [a,b], Gábor L. Katona [a,*]

[a] Department of Solid State Physics, Faculty of Sciences and Technology, University of Debrecen, P.O. Box 400, H-4002, Debrecen, Hungary
[b] University of Debrecen, Doctoral School of Physics, Debrecen, Hungary

ARTICLE INFO

Keywords:
FePd
FePdAu
Buffer layers
$L1_0$ ordering
$L1_2$ ordering
Multilayer

ABSTRACT

Fe-Pd based thin films with Au intermediate layer fabricated on different substrates (SiO_2, SiO_2/Mo, SiO_2/W) were investigated at annealing temperatures up to 460 °C. The samples were deposited by magnetron sputtering and were post-annealed in vacuum. The ongoing processes were investigated by chemical depth profiling and X-ray diffraction. The experimental results showed that the intermediate Au layer always promoted the formation of $FePd_3$ phase which also showed $L1_2$ ordered structure except in one case with W underlayer. However, in the samples with Mo buffer but without the Au interlayer the FePd phase formed and $L1_0$ ordered phase also appeared for one stacking order. Considering the low diffusivity arising from the annealing temperature the processes were explained by grain boundary diffusion induced reaction layer formation. The formation of the ordered FePd phases was interpreted by the stress accumulation due to the different diffusivity of the components, which relaxes by the shift of the grain boundaries and the transformation of swept over regions. It was concluded, that the effect of the Au interlayer is dominant over the effect of the Mo or W buffer layers.

1. Introduction

Fe-Pd thin films are promising materials since they are characterized by favourable magnetic properties making them suitable for technical applications like magnetic recording or spintronics [1–3]. These properties, like high saturation magnetization, high magnetocrystalline anisotropy and coercive field are usually related to the crystallographic structure i.e. the presence of an ordered $L1_0$ phase. From this group of magnetic materials the Fe-Pt is far the most investigated, but the Fe-Pd based system is also interesting and important since it could be used to cost effectively produce suitable layers.

There are several possible ways for producing the tetragonal ordered phase in Fe-Pt, e.g. bi-/multilayer deposition or codeposition on different substrates [4], applying heated substrates during deposition [5], high temperature annealing after deposition [6], annealing in different atmospheres [7], utilizing buffer and seed layers [6,8–10], or adding a third component to the system [11–14]. All of the processes listed above can promote the formation of the ordered phase and can even reduce the formation temperature of it.

Similar approaches have also been investigated in Fe-Pd. Layer deposition on heated substrates and/or performing high temperature post-annealings can lead to the formation of the $L1_0$-FePd phase [15–17]. Bahamida et al. [16] investigated the transformation

* Corresponding author.
E-mail address: gabor.katona@science.unideb.hu (G.L. Katona).

https://doi.org/10.1016/j.heliyon.2024.e32865
Received 31 March 2024; Received in revised form 10 June 2024; Accepted 11 June 2024

Available online 14 June 2024

of $Fe_{56}Pt_{44}$ alloys at 550 °C and have found, that although the transformation is relatively rapid at this temperature, the further structural evolution of the ordered phase has significant impact on film properties. Layer deposition at 200 °C and then post annealing at 600 °C resulted in the formation of the ordered $L1_0$ phase [18]. Utilizing different buffer layers can also enhance the formation of $L1_0$-FePd phase and decrease the formation temperature [19–22]. Chang et al. have found [19] that W underlayer on glass substrate has promoted the formation of ordered phase in 50 nm FePd films. Li et al. applied Ag as underlayer [21] for a multilayered Fe/Pd thin film on glass substrate. They have found that the ordering temperature was reduced. However, in this case the underlayer was not inert, as the Ag diffused into the film which effectively promoted the formation of $L1_0$ ordered phase.

Deposition on suitable oriented substrates can also be used to form ordered FePd phase [23]. It has been found that formation of the $L1_0$ phase is significantly promoted when an amorphous CoFeB intermediate layer is inserted between the FePd layer and the MgO substrate [24]. Wang et al. [25] have found that the applied buffer layer can influence not only the forming phase but also the magnetic properties of the material. They observed that application of Ir, Cr/Ir, Cr/Pt, Cr/Rh or Cr/Ru buffer layers inserted under FePd films can induce the formation of ordered $L1_0$ phase during annealing while Mo/Ir underlayer does not. Annealing in atmosphere containing H_2 also influences these processes and results in improvement of magnetic properties [26–28].

Addition of a third component can also be an effective way to produce the ordered phase [21,23,29–34]. Polit et al. discussed the effect of Cu on the formation FePd phase [30]. They have post-annealed {Cu/Fe/Pd}×5 multilayer thin films at high temperature with rapid thermal annealing. It was found that ordered ternary FePdCu alloy formed and they could also improve the (001) texture with additional annealing. Perzanowski et al. have investigated Cu/Fe/Pd multilayers annealed by rapid thermal annealing and by conventional long annealing on various substrates [32]. They have found, that FePd:Cu thin alloy films formed and the MgO(100) and Si(100) substrates were the most suitable for ordered and (001) textured films. The same authors also applied pulsed laser annealing to Cu/Fe/Pd multilayers [33], which led to formation of partially ordered FePdCu nanocrystallites. Myagkov et al. [31] have investigated the effect of a thick Ag interlayer. They have found that the presence of Ag enhanced the formation of the ordered $L1_0$ phase, despite the thickness of the Ag layer. Tokuoka et al. have also investigated the effect of Ag [23] with 5 nm FePd/Ag and FePt/Ag films grown on MgO(001) substrate. They have found, that FePt and FePd behave differently, as in case of FePt the Ag addition effectively promoted the $L1_0$ ordering, while in case of FePd the effect was smaller. Zhang et al. found [34] that an Ag toplayer on FePd thin film effectively promotes the transformation from disordered fcc to ordered fct structure.

It is an interesting and from practical applications point of view also important question whether the formation of ordered $L1_0$-FePd phase can be achieved at lower temperatures. In this paper we have investigated the effect of Au interlayer, and also the effect of non-interacting Mo and W buffer layers on the formation of new phases in Fe/Pd thin films at relatively low temperatures. The aim is to determine whether an Au interlayer or Mo and W buffer layers are suitable to promote the formation of the magnetically favourable $L1_0$ FePd phase.

2. Experimental

Three-component layered films were prepared by DC magnetron sputtering on thermally oxidized Si/SiO_2(100 nm) substrates at room temperature using individual Fe, Au and Pd targets. The deposition rate was 0.1 nm/s for Fe, and 0.12 nm/s for Au and Pd. The nominal structure of the samples were the following (Fig. 1):

S1 (Fig. 1a): SiO_2/Fe(15 nm)/Au(10 nm)/Pd(22 nm)

S2 (Fig. 1b): SiO_2/Pd(18 nm)/Au(10 nm)/Fe(15 nm)/Pd(4 nm)

The thickness of Fe (15 nm) and Pd (22 nm) results in a nominal composition of 45 at% Fe and 55 at% Pd, considering only Fe and Pd, which falls into the existence range of the FePd phase.

We have also fabricated samples with and without Au interlayer using a 20 nm thick sputter deposited Mo buffer layer on top of Si/SiO_2 as substrate. The deposition rate of Mo was 0.13 nm/s. The nominal structure of the samples were (Fig. 1):

S3 (Fig. 1c): SiO_2/Mo(20 nm)/Fe(15 nm)/Pd(22 nm)

S4 (Fig. 1d): SiO_2/Mo(20 nm)/Pd(18 nm)/Fe(15 nm)/Pd(4 nm)

S5 (Fig. 1e): SiO_2/Mo(20 nm)/Fe(15 nm)/Au(10 nm)/Pd(22 nm)

S6 (Fig. 1f): SiO_2/Mo(20 nm)/Pd(18 nm)/Au(10 nm)/Fe(15 nm)/Pd(4 nm)

In case of sample S2, S4 and S6 the Pd layer was divided in two in order to provide a thin Pd cap layer to reduce the oxidation of the Fe. The overall composition were the same for the S1-S2, S3-S4 and S5-S6 pairs, respectively. Samples S5 and S6 were also prepared in a variant using W as buffer layer. The samples were annealed in high vacuum (10^{-7} mbar). During annealing the samples were heated up to the desired temperature with a heating rate of ~20 °C/min. At the end of the heat treatment the system was let cool down under vacuum without external control with a cooling rate of ~15 °C/min in the first 150 °C temperature drop. It is important to note that each annealing was performed on an as deposited sample and the annealings are not parts of a sequence carried out on the same sample. In order to investigate the ongoing diffusion processes and the evolution of depth distribution of the components chemical depth profiling was performed on the as deposited and post annealed samples using Secondary Neutral Mass Spectrometry (SNMS, INA-X from SPECS GmbH) in direct bombardment mode. The source of the bombarding ions was a RF Ar plasma and the sputtering area was 3 mm in diameter. The measured intensity profiles were converted into composition profiles

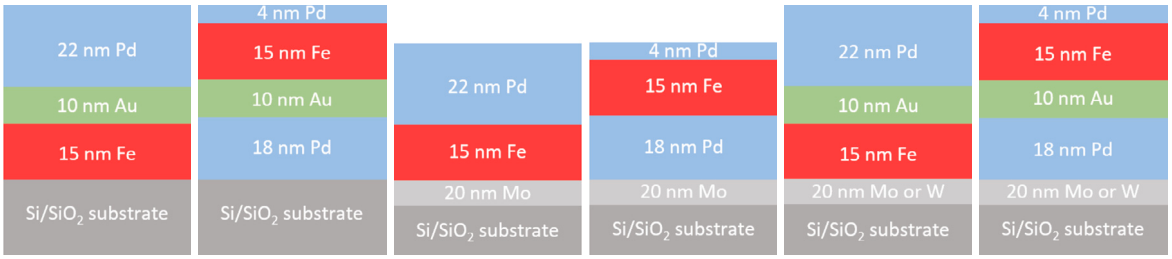

(a) S1 (b) S2 (c) S3 (d) S4 (e) S5 (f) S6

Fig. 1. Schematic drawings of the nominal structures of the as deposited samples.

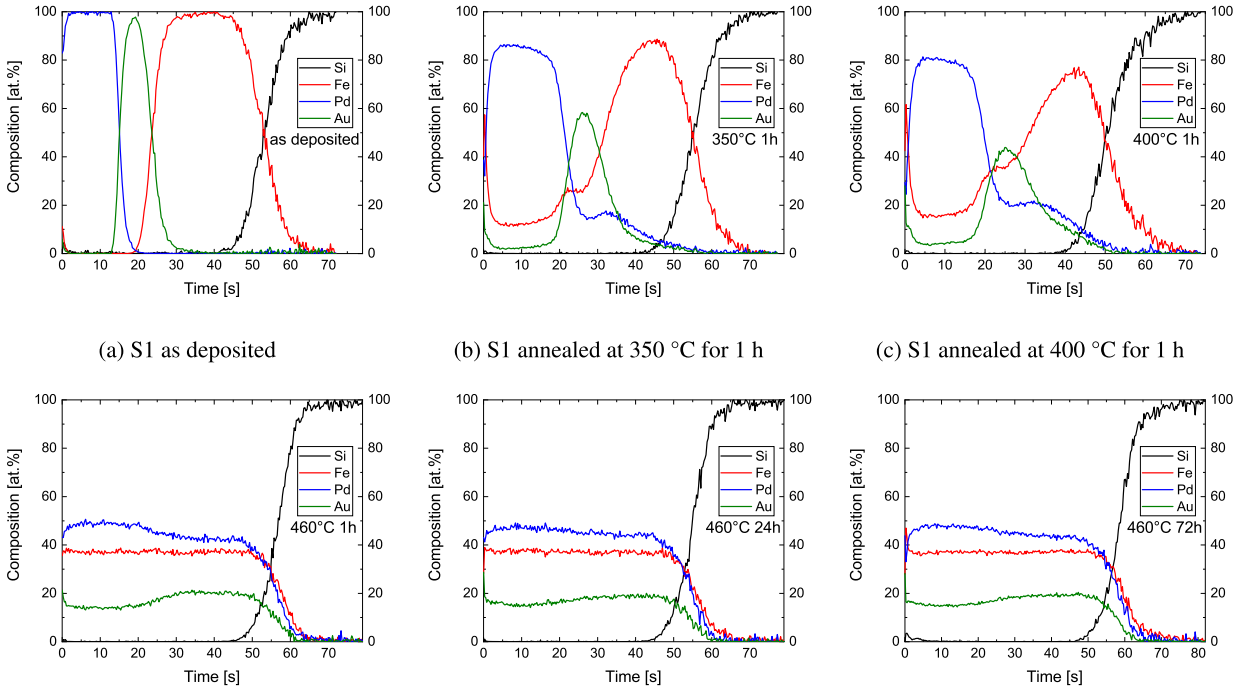

(a) S1 as deposited (b) S1 annealed at 350 °C for 1 h (c) S1 annealed at 400 °C for 1 h

(d) S1 annealed at 460 °C for 1 h (e) S1 annealed at 460 °C for 24 h (f) S1 annealed at 460 °C for 72 h

Fig. 2. Composition depth profiles of the SiO_2/Fe(15 nm)/Au(10 nm)/Pd(22 nm) (S1) sample after various annealings.

assuming linear dependence of intensities on concentration under stationary sputter conditions. Structural properties were studied by X-ray Diffraction (XRD, Rigaku SmartLab II) in $\theta - 2\theta$ geometry using Cu Kα radiation.

3. Results

3.1. Effect of Au interlayer

In case of the S1 and S2 samples we have carried out 1 h isochronal annealing at 350 °C, 400 °C and 460 °C and also isothermal annealing at 460 °C for 1, 24 and 72 h. Considering the volume diffusion coefficients of the components at these temperatures volume diffusion is not expected. The composition depth profiles of the samples are shown in Fig. 2 and Fig. 3, while Fig. 4 and Fig. 5 show the corresponding XRD patterns for S1 and S2, respectively.

Looking at the depth profiles of the as deposited samples we can see that there are relatively sharp interfaces between the individual layers in case of both stacking order (Figs. 2a and 3a) corresponding well to the instrumental broadening of the technique. The XRD patterns show pure Fe, Pd and Au reflections (Figs. 4a and 5a). It should be noted, that the texture of the Pd and Fe layers differ in the two samples. While the Pd layer is not textured in case of S1 according to the intensity ratio of the Pd(111) and Pd(200) reflections, the S2 sample shows a preferred (111) orientation. Similarly the structure of the Fe layer also differs because Fe has an intensive (110) reflection for the S1 sample, but only a weak one in case of S2.

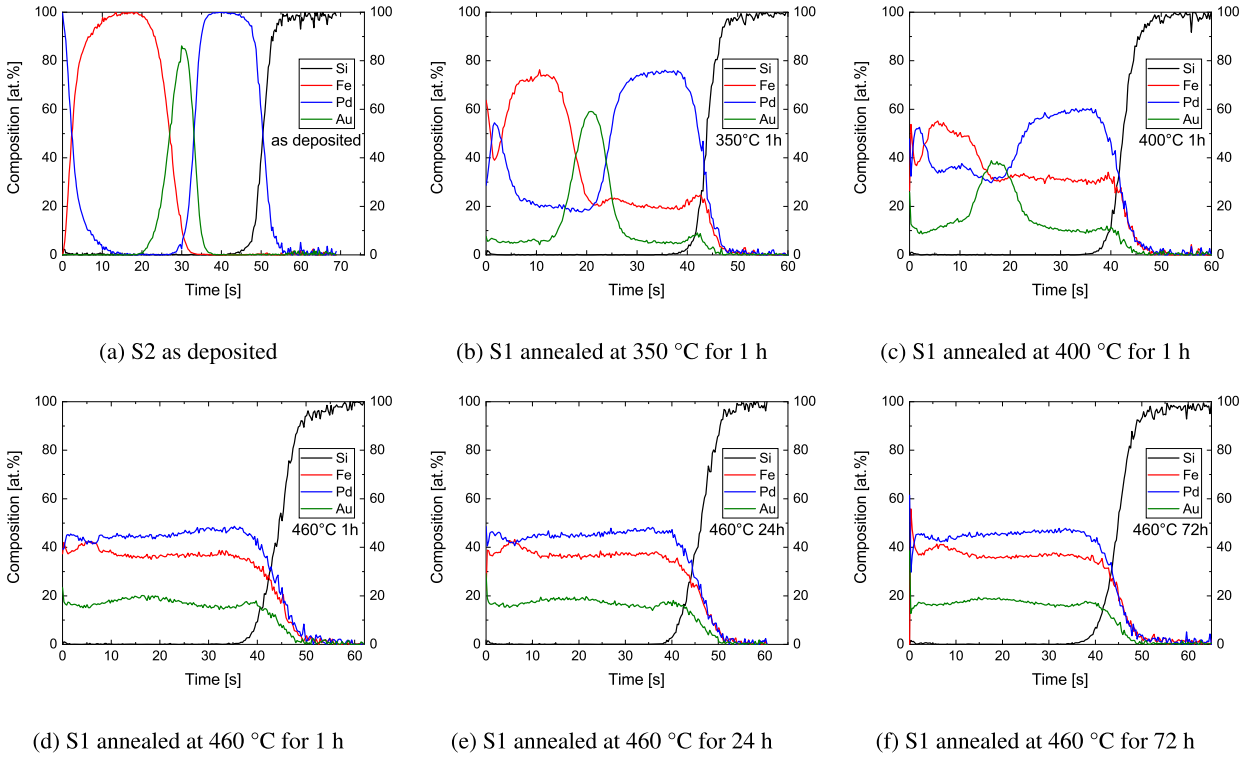

(a) S2 as deposited (b) S1 annealed at 350 °C for 1 h (c) S1 annealed at 400 °C for 1 h

(d) S1 annealed at 460 °C for 1 h (e) S1 annealed at 460 °C for 24 h (f) S1 annealed at 460 °C for 72 h

Fig. 3. Composition depth profiles of the SiO_2/Pd(18 nm)/Au(10 nm)/Fe(15 nm)Pd(4 nm) (S2) sample after various annealings.

Annealing at 350 °C for 1 h results in mutual penetration of Fe and Pd into each other through the Au layer for both samples (Figs. 2b and 3b). In case of S2 the intermixing is symmetrical; i.e. the Fe and Pd concentration is approximately the same and constant with depth in both layers (approx. 20 at%) and also in the Au layer. At the same time the Fe and Pd layers have the same Au content in the full thickness with minor Au segregation to the substrate. Contrary to this S1 shows less intensive intermixing: lower Pd and Fe content in each other than in S2 (approx. 12 at% Fe in Pd and somewhat less Pd in Fe) and in the Fe layer the Pd (and also the Au) distribution is not homogeneous. A plausible explanation for this is the different structure of layers as can be seen in the corresponding as deposited XRD patterns (Figs. 4a and 5a), which can change the possible diffusion pathways. XRD patterns of the first annealing step (Figs. 4b and 5b) show the disappearance of individual Fe and Au reflections and the presence of AuPd peaks. The difference in texture is also present in case of the freshly formed AuPd phases. While in S1 both the AuPd(111) and the AuPd(200) reflections appear, the S2 sample shows strong texture as only the AuPd(111) reflection is detected with much higher relative intensity compared to the Pd(111) reflection. In case of S1 the Pd reflections are also somewhat shifting toward to the right in direction of FePd phases (FePd and $FePd_3$).

Annealing at higher temperature for the same duration (400 °C 1 h) the intermixing is more developed, the Au and Fe content of the Pd layer is increasing for both samples and also inside the Fe layer there is increased amount of Pd and Au. In case of sample S1 the Au and Pd content in the Fe layer are almost the same and both are decreasing with depth (Fig. 2c), similarly to the lower temperature annealing. In the reverse order S2 sample the Au, Pd and Fe content of each layer are still reasonably higher than in S1 and the distribution of all diffusing species in the other layers is homogeneous (Fig. 3c) just like in the previous step. On the XRD patterns (Figs. 4c and 5c) we can see that in both samples the relative intensities of the AuPd reflections are decreased, in case of S1 the originally present AuPd(200) is almost completely disappeared. The reflection close to 41° in S1 indicates the formation of FePd phases (Fig. 4c).

Annealing at 460 °C for 1 h results in intensive intermixing for both S1 and S2; the depth profiles (Figs. 2d and 3d) show almost homogeneous depth distributions of the components. The initial layered structure became almost undetectable in case of S2, although the Au depth distribution still suggests the position of the original Au layer. In contrast to this the Au depth profile of S1 shows two distinct regions corresponding to the original Pd and Fe layers with higher Au content at the place of the initial position of the Fe layer. At the same time on the XRD patterns only the reflections belonging to $FePd_3$ phase are visible in both samples (Figs. 4d and 5d). It should be noted that the $FePd_3$ phase has a wide composition range, thus the indicated positions can change with composition and also because of the possible stress arising in the system. Additionally new peaks become visible on the XRD patterns. For both samples the $FePd_3$(100) reflection appears indicating ordering of the $FePd_3$ phase. In case of S1 the $FePd_3$(110) peak also becomes detectable. It should be noted that the $FePd_3$(100) reflection has lower relative intensity in case of the originally more textured S2 sample.

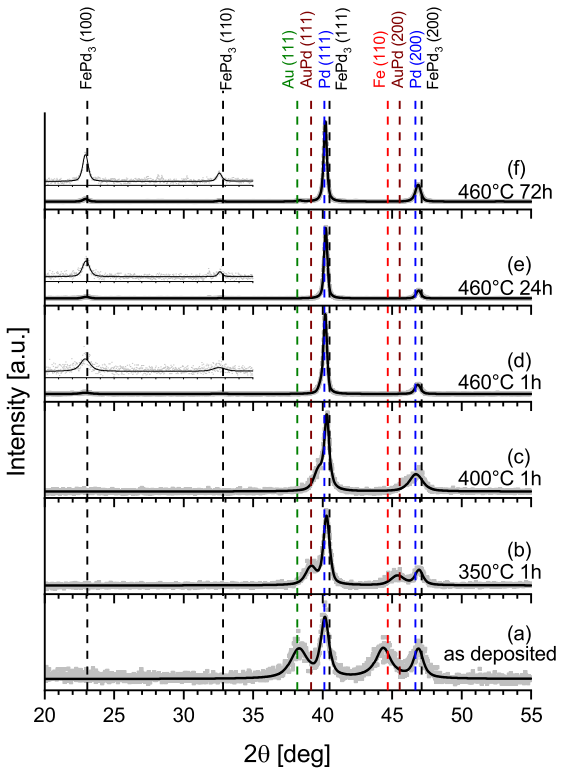

Fig. 4. XRD patterns of SiO_2/Fe(15 nm)/Au(10 nm)/Pd(22 nm) (S1) sample after various annealings. The magnification of the insets is 10x.

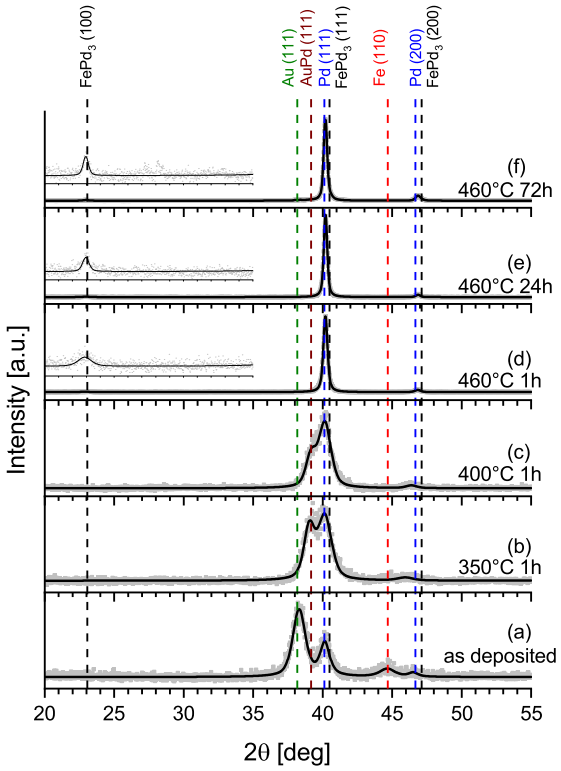

Fig. 5. XRD patterns of SiO_2/Pd(18 nm)/Au(10 nm)/Fe(15 nm)/Pd(4 nm) (S2) sample after various annealings. The magnification of the insets is 30x.

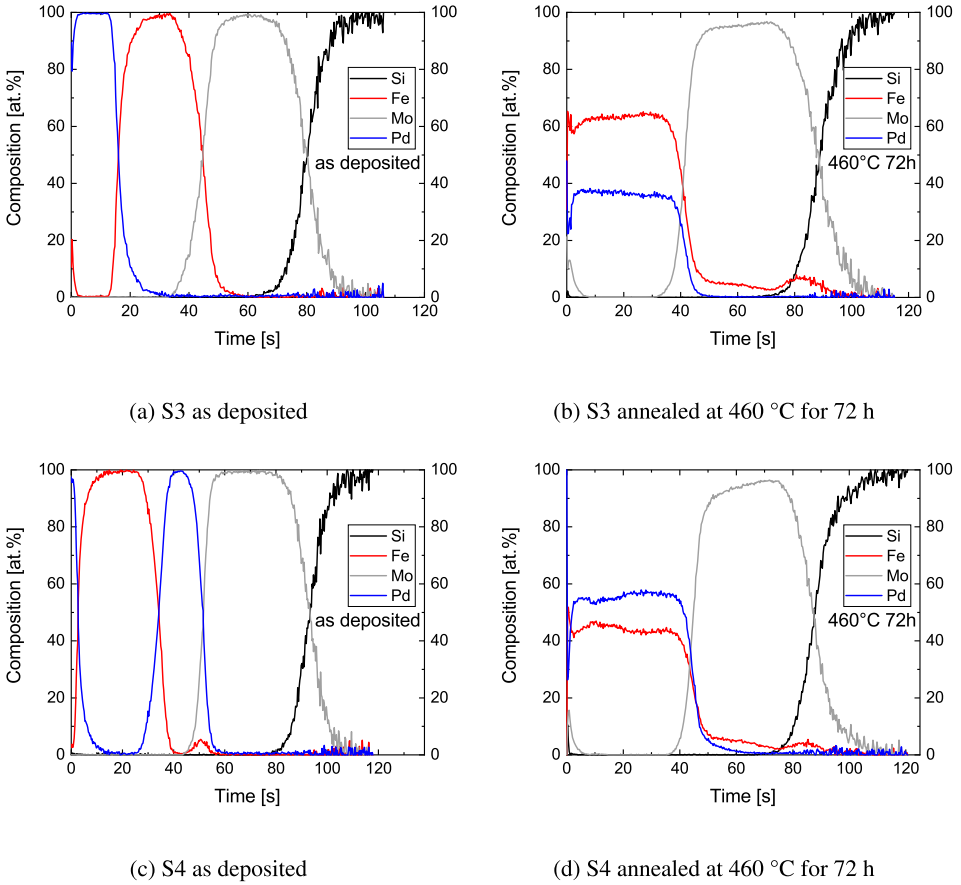

(a) S3 as deposited

(b) S3 annealed at 460 °C for 72 h

(c) S4 as deposited

(d) S4 annealed at 460 °C for 72 h

Fig. 6. Composition depth profiles of the S3: SiO_2/Mo(20 nm)/Fe(15 nm)/Pd(22 nm) and S4: SiO_2/Mo(20 nm)/Pd(18 nm)/Fe(15 nm)/Pd(4 nm) samples.

In order to see how the structure develops upon longer annealings and to check the stability of the formed $FePd_3$ phase, we kept the temperature at 460 °C and made isothermal annealing for 24 h and 72 h. The composition-depth profiles show that longer annealing results in the smoothing of the distribution of the constituents; i.e. the depth profiles become more homogeneous. The XRD patterns show the presence of $FePd_3$ phase and also increasing intensity of the (100) and (110) $FePd_3$ superlattice reflections which clearly indicates the presence of the ordered $L1_2$-$FePd_3$ phase in case of both samples.

3.2. Effect of Mo buffer layer

It was found previously that in case of bilayered Fe/Pd samples fabricated on Si/SiO_2(100 nm) substrate the $FePd_3$ phase was formed after similar annealings [35]. In order to promote the formation of $L1_0$-FePd phase we have prepared bilayered samples using a 20 nm thick Mo buffer layer on top of Si/SiO_2 substrate with the following structure (see also Experimental):

S3: SiO_2/Mo(20 nm)/Fe(15 nm)/Pd(22 nm)

S4: SiO_2/Mo(20 nm)/Pd(18 nm)/Fe(15 nm)/Pd(4 nm)

Annealing at 460 °C for 72 h was carried out on these samples to reach a well developed state. The depth profiles of the as deposited samples show well separated layers (Figs. 6a and 6c) and the XRD patterns (Figs. 7a and 7c) are also quite similar with reflections of Pd(111) and Pd(200), Fe(110) and Mo(110). The reflections of Pd show a heavily textured structure in both samples based on the intensity ratio of Pd(111)/Pd(200).

After annealing the depth profiles still show a layered structure, but with only two layers, since the annealing resulted in complete homogenization of the Fe and Pd layers while the Mo layer is practically unaffected as a consequence of very low diffusion coefficient, only a small amount of Fe and Pd appear in the Mo layer with minor Fe segregation to the layer/substrate interface. The Fe and Pd in the Mo layer should be located at the grain boundaries taking into account the phase diagrams and the low annealing temperature. Looking first at the XRD pattern of sample S4 the presence of the FePd phase is indicated by the detection of the FePd(001), FePd(111), FePd(200) and FePd(002) reflections. The appearance of the FePd(200) and FePd(002) reflections indicates tetragonal splitting. The presence of the FePd(001) reflection shows that the structure is also partially ordered in addition to the tetragonal transformation. This means, that in sample S4 an ordered $L1_0$-FePd phase has been formed. In contrast to this in sample S3 only

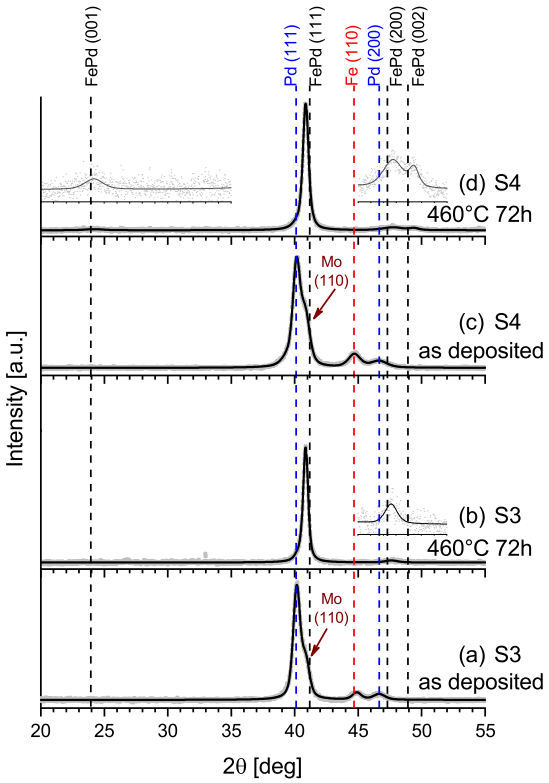

Fig. 7. XRD patterns of as deposited and annealed S3: SiO_2/Mo(20 nm)/Fe(15 nm)/Pd(22 nm) and S4: SiO_2/Mo(20 nm)/Pd(18 nm)/Fe(15 nm)/Pd(4 nm) samples. The magnification of the insets is 10x.

FePd(111) and FePd(200) reflections appear after annealing, the FePd(001) and FePd(002) reflection are not detected. Comparing the position of the (200) reflection of the formed phase with the pattern of sample S4 it can be concluded, that in S3 also the FePd phase forms, however for this stacking without ordering. In case of sample S4 we have performed shorter annealing for 8 h at 460 °C (not shown) where the composition depth profile was not homogeneous, but the XRD pattern already showed the appearance of the ordered phase.

Since the Mo buffer layer promoted the formation of the $L1_0$ ordered phase in case of Fe/Pd bilayers we have created samples using a Mo(20 nm) buffer layer and Au additive; i.e. we have combined the previous sample structures in order to check if the Mo underlayer also enhance the formation of the ordered FePd phase in the FeAuPd system. The nominal structure of these samples were the following (see also Experimental):

S5: SiO_2/Mo(20 nm)/Fe(15 nm)/Au(10 nm)/Pd(22 nm)

S6: SiO_2/Mo(20 nm)/Pd(18 nm)/Au(10 nm)/Fe(15 nm)/Pd(4 nm)

The samples were annealed again for 72 h at 460 °C. The corresponding composition depth profiles are shown in Fig. 8. The as deposited samples show a well resolved layered structure just as in the case of the previous samples (Figs. 8a and 8c). The annealing results in an almost completely homogeneous composition distribution with depth regarding of the Fe, Au and Pd components in both samples (Figs. 8b and 8d). The Mo buffer layer is only slightly affected similarly to the previous case, mostly Fe appears in the layer and the detected compositions in the Mo correspond to filling up of the grain boundaries. Additionally minor Fe segregation can be seen at the SiO_2/Mo interface. The XRD pattern of the as deposited samples is shown in Figs. 9a and 9c, where reflections from Fe, Pd, Au and Mo appear. Looking at the XRD patterns of the annealed samples (Figs. 9b and 9d) formation of $FePd_3$ phase can be seen in both cases, as indicated by the appearance of the $FePd_3$ (111) and (200) reflections, while the reflections of the individual components vanish completely. Additionally for both samples the $FePd_3$(100) and for S5 also the $FePd_3$(110) superlattice reflections become detectable, indicating the formation of ordered $FePd_3$ phase. It should be noted, that the (100) reflection is sharper and has higher relative intensity in case of S6 showing a more developed ordering state. The results show that while the Mo buffer layer alone promotes the growth of the FePd phase, combining it with Au interlayer results in formation of $FePd_3$ phase.

In order to check if a buffer layer of different material can promote the formation of the FePd phase instead of $FePd_3$ in the three-component FeAuPd system the Mo underlayer were replaced with a 20 nm thick W layer in S5 and S6. We have found (results not shown) after the same annealing that the W buffer layer stayed intact just as in case of the Mo buffer

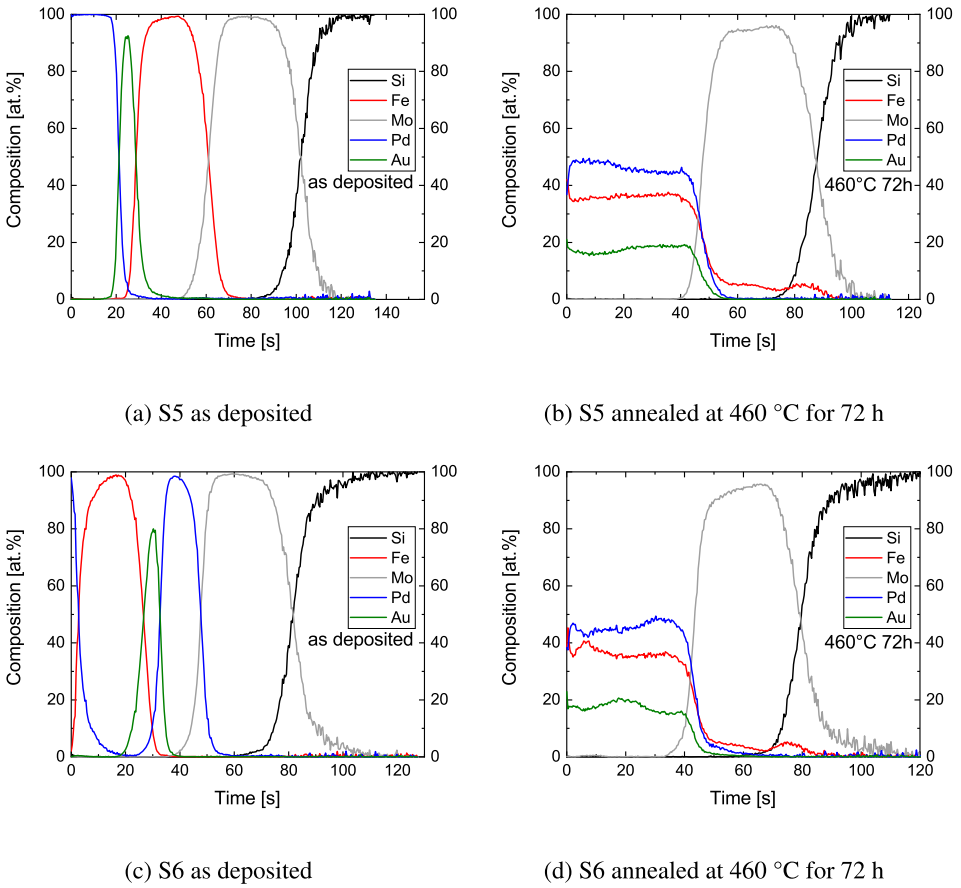

(a) S5 as deposited (b) S5 annealed at 460 °C for 72 h

(c) S6 as deposited (d) S6 annealed at 460 °C for 72 h

Fig. 8. Composition depth profiles of the as deposited and annealed S5: SiO_2/Mo(20 nm)/Fe(15 nm)/Au(10 nm)/Pd(22 nm) and S6: SiO_2/Mo(20 nm)/Pd(18 nm)/Au(10 nm)/Fe(15 nm)/Pd(4 nm) samples.

Table 1
Comparison of phases formed after annealing at 460 °C for 72 h. Samples marked with star (*) are from [35].

System	SAMPLE STRUCTURE		Forming phase			
			A1-FePd	$L1_0$-FePd	A1-$FePd_3$	$L1_2$-$FePd_3$
FePd	SiO_2/	Fe/Pd*			✓	
		Pd/Fe/Pd*				✓
	SiO_2/Mo/	Fe/Pd	✓			
		Pd/Fe/Pd		✓		
FeAuPd	SiO_2/	Fe/Au/Pd				✓
		Pd/Au/Fe/Pd				✓
	SiO_2/Mo/	Fe/Au/Pd				✓
		Pd/Au/Fe/Pd				✓
	SiO_2/W/	Fe/Au/Pd				✓
		Pd/Au/Fe/Pd			✓	

and it did not lead to different phase. We have detected $FePd_3$ for both stacking orders, which was ordered only in case of SiO_2/W(20 nm)/Fe(15 nm)/Au(10 nm)/Pd(22 nm).

The obtained phases after annealing at 460 °C for 72 h are summarized in Table 1. As it can be seen, in most cases the $FePd_3$ phase is formed.

4. Discussion

An important common feature of all presented results is the full homogenization of the films despite the relatively low annealing temperature. At this temperature volume diffusion is essentially negligible, since according to diffusion coefficients [36] the volume diffusion penetration depth is below 1 nm at 460 °C for 72 h. This means, that the mixing of the layers and also the formation of

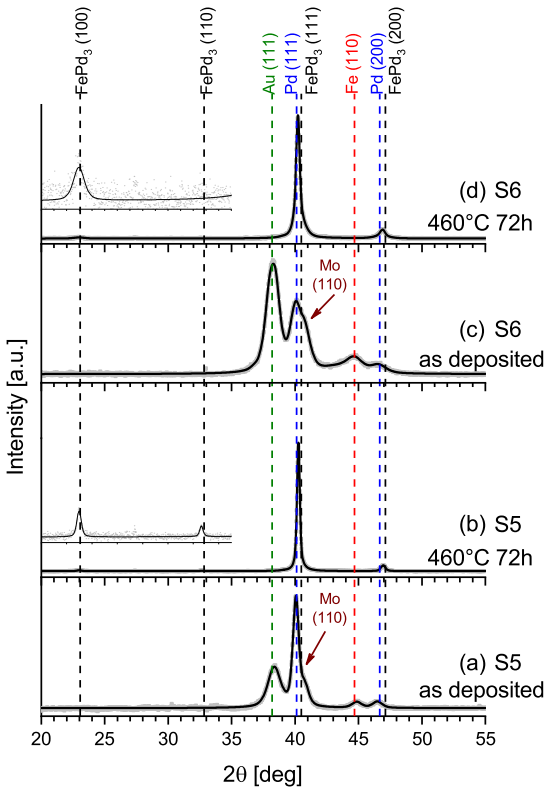

Fig. 9. XRD patterns of as deposited and annealed S5: SiO_2/Mo(20 nm)/Fe(15 nm)/Au(10 nm)/Pd(22 nm) and S6: SiO_2/Mo(20 nm)/Pd(18 nm)/Au(10 nm)/Fe(15 nm)/Pd(4 nm) samples. The magnification of the insets are 30x.

the new (ordered) phases cannot occur by volume diffusion. This is also supported by the step-by-step results of S1 and S2, where in case of annealings at lower temperatures (for shorter times) it is visible in the depth profiles that the mixing of the films did not start from the interfaces and then gradually proceeded via reaction layer formation at the original interfaces to fully mix the system, but happened parallel in the whole thickness (volume) of the layers which is clearly different from the usual growth mode. This phenomenon was observed recently in several thin film systems, like AuCu [37,38], CuPd [39], FePt [12,13].

These observations can be interpreted by grain boundary diffusion and connected mechanisms. It is known, that during grain boundary diffusion the grain boundary can migrate, leaving behind an alloyed region. This phenomenon is called Diffusion Induced Grain Boundary Migration (DIGM) [40–46]. Since grain boundary (GB) diffusion is fast even at the investigated temperature, this explains why the mixing occurs in the whole thickness of the film.

Recently it was shown [43], that during DIGM in suitable materials in which ordered phases exist it can happen, that the alloyed region is not a solid solution of the mixed components, but ordered phases can also form. This is called Grain Boundary Diffusion Induced Reaction Layer Formation (GBDIREAC). This is a key phenomenon in the understanding of the observed low temperature formation of the $L1_0$-FePd and $L1_2$-$FePd_3$ phases. At the beginning of the process the diffusing components migrate along GBs and accumulation at the interfaces and free surface occurs. These enrichments will themselves become diffusional sources which means, that there will be diffusion of atoms from both sides of each layer. This will lead to a close to homogeneous filling up of the layers with the atoms from other layers. The interdiffusion along GBs results in the formation of a stress field, which can stop interdiffusion or can be relaxed by the shift of the GBs. During this movement new phases grow along the GBs. This shift of the boundaries leads to the intermixing of the originally separated components and also to the formation of ordered phases if there is a suitable chemical driving force [43].

Looking at the detailed annealing steps of sample S1 and S2 the above interpretation can be adopted as follows. In the first annealing steps of S1 it can be seen, that the Fe and Au diffuse into the Pd layer and accumulate at the free surface of Pd. Together with this enrichment at the surface the Fe and Au almost homogeneously fill up the Pd layer. The Au layer is similarly filled up by Fe and Pd atoms. From the XRD patterns it can be concluded, that the Pd even forms an intermediate AuPd phase with the Au. In case of the Fe layer the Pd composition is not homogeneous as compared to the Fe composition in the Pd layer. This can be interpreted with the lower diffusion coefficient of Pd in the Au grain boundaries. In case of S2 the process is very similar regarding of the Pd and Au layers and the segregation (as a result of rapid diffusion along the fastest GBs) of Fe and Au at the film/substrate interface is clearly visible. Correspondingly the composition of Fe and Au is increasing in the Pd layer in its whole thickness just as in the Au layer since both layers have sources of diffusing atoms on both sides. Contrary to sample S1 in this case the Fe layer is also filled up similarly to the Pd layer. This is mainly the consequence of the Pd cap layer acts as a source of Pd from the beginning of the process,

thus although the diffusion of Pd is slower along the Au grain boundaries than that of the Fe diffusion, but this top layer echances the process of filling up the Fe layer. The difference in the Au distribution can be accounted to the difference in the layer structure as it can be seen from the XRD pattern of the as deposited samples. The process finally leads to consumption of the individual layers. Since the underlying process is grain boundary diffusion, the mixing of the layers and the formation of new phases can be understood by the aforementioned shift and migration of the GBs which then leave behind mixed regions with new, partially ordered phases. The same interpretation can be used for the diffusion processes in case of the other samples with Mo and W buffer layers. The effect of the Mo buffer layer on the two-component (Fe-Pd without Au interlayer) films is in accordance with previous results [20], where Mo buffer also promoted the formation of $L1_0$-FePd phase. This is plausibly the effect of the different lattice constant which introduces stress in the layers. Similarly to the FePt system [47,48] this can promote the ordering of the FePd phase. Differences in diffusion and stress effects are the plausible explanation for the effect of the Au layer which always promotes the formation of $FePd_3$ phase. The diffusion of Fe and Pd through the Au grain boundaries are different as it was shown, which introduces an additional stress in the system. In this case because the inequality of the diffusion fluxes there will be tensile and compressive stress in the Fe and Pd layers, respectively. This effect of this stress dominates over the stress arised because of the different substrates.

It is worth comparing our results to those obtained in the FePt system. In case of the FePt system in a sample with almost equiatomic Fe and Pt content without additional components there are no reports on other than $L1_0$-FePt phase formation. Addition of Au to such almost equiatomic Fe/Pt thin film did not change this behaviour, only the formation temperature and other properties changed [13,14,47,49]. In contrast to this in case of the FePd system in a similarly fabricated close to equiatomic two-component system the $FePd_3$ phase forms which is further promoted by the addition of Au; i.e. in samples with Au addition the formation of ordered phase takes less time as compared to the two-component system. As we have shown, introducing a Mo buffer layer effectively promotes the formation of FePd phase in case of two component samples (samples S3 and S4) which is even ordered for one stacking order (sample S4). Comparing this with samples S5 and S6, which have Au added besides the Mo buffer layer it can be seen, that effect of Au is dominant over the effect of the Mo buffer layer, because in these samples ordered $FePd_3$ phase forms. Utilizing W underlayer instead of Mo in the FeAuPd system also promoted the formation of $FePd_3$ phase which showed ordering for one stacking order.

5. Conclusion

Different Fe-Pd based thin film structures were investigated in order to check the effect of an intermediate Au layer and different buffer layers (Mo, W) on the structural and phase transformations during low temperature annealings. We have shown, that despite the low annealing temperature it is possible to form new phases and applying an intermediate Au layer clearly determines the forming new phase. The volume diffusivity of the components at the applied annealing temperatures is low and the step-by-step depth profiles showed that the mixing between the components occurred in the whole volume of the film without reaction front starting from the layer interfaces. Considering these we have interpreted the intermixing and the formation of new phases by grain boundary diffusion assisted mechanisms: diffusion induced grain boundary migration (DIGM) and grain boundary diffusion induced reaction layer formation (GBDIREAC). Our results show that applying a Mo underlayer to the two-component Fe-Pd samples promoted the formation of the FePd phase, which showed $L1_0$ ordering for one stacking order. In contrast with this in case of samples containing Au intermediate layer in all cases the $FePd_3$ phase formed irrespective of whether buffer layer was applied or not. The formed phase was always ordered except for one stacking sequence grown on W buffer layer. This suggests that the presence of Au has a stronger influence of the ongoing phase transformations in the system than the buffer layers which was accounted to stress effects.

CRediT authorship contribution statement

Szilvia Gulyás: Writing – review & editing, Writing – original draft, Visualization, Methodology, Investigation, Formal analysis, Data curation, Conceptualization. **Gábor L. Katona:** Writing – review & editing, Writing – original draft, Validation, Supervision, Resources, Methodology, Investigation, Formal analysis, Conceptualization.

Declaration of competing interest

The authors declare that they have no known competing financial interests or personal relationships that could have appeared to influence the work reported in this paper.

Data availability

Data will be made available on request.

References

[1] D. Weller, O. Mosendz, G. Parker, S. Pisana, T.S. Santos, $L1_0$ FePtX-Y media for heat-assisted magnetic recording, Physica Status Solidi (A) Applications and Materials Science 210 (7) (2013) 1245–1260.

[2] D. Weller, G. Parker, O. Mosendz, A. Lyberatos, D. Mitin, N.Y. Safonova, M. Albrecht, Review article: FePt heat assisted magnetic recording media, Journal of Vacuum Science & Technology B, Nanotechnology and Microelectronics: Materials, Processing, Measurement, and Phenomena 34 (6) (2016) 060801, https://doi.org/10.1116/1.4965980.

[3] Y. Xu, D.D. Awschalom, J. Nitta (Eds.), Handbook of Spintronics, Springer, Netherlands, Dordrecht, 2016.

[4] T. Bublat, D. Goll, Temperature dependence of the magnetic properties of $L1_0$-FePt nanostructures and films, J. Appl. Phys. 108 (11) (2010) 113910, https://doi.org/10.1063/1.3512906.

[5] T. Shima, T. Moriguchi, S. Mitani, K. Takanashi, Low-temperature fabrication of $L1_0$ ordered FePt alloy by alternate monatomic layer deposition, Appl. Phys. Lett. 80 (2) (2002) 288–290, https://doi.org/10.1063/1.1432446.

[6] H. Zeng, M.L. Yan, N. Powers, D.J. Sellmyer, Orientation-controlled nonepitaxial $L1_0$ CoPt and FePt films, Appl. Phys. Lett. 80 (13) (2002) 2350–2352, https://doi.org/10.1063/1.1464663.

[7] I.A. Vladymyrskyi, M.V. Karpets, F. Ganss, G.L. Katona, D.L. Beke, S.I. Sidorenko, T. Nagata, T. Nabatame, T. Chikyow, G. Beddies, M. Albrecht, I.M. Makogon, Influence of the annealing atmosphere on the structural properties of FePt thin films, J. Appl. Phys. 114 (16) (2013) 164314, https://doi.org/10.1063/1.4827202.

[8] B.C. Lim, J.S. Chen, J.F. Hu, Y.K. Lim, B. Liu, G.M. Chow, G. Ju, Improvement of chemical ordering of FePt (001) oriented films by MgO buffer layer, J. Appl. Phys. 103 (7) (2008) 07E143, https://doi.org/10.1063/1.2835089.

[9] T. Suzuki, Nanostructured $L1_0$ Fe-Pt based thin films for perpendicular magnetic recording, Mater. Trans. 44 (8) (2003) 1535–1541, https://doi.org/10.2320/matertrans.44.1535.

[10] J.-L. Tsai, Q.-S. Luo, P.-R. Chen, Y.-T. Tseng, Magnetic properties and microstructure of FePt/MoC/CrRu films, J. Magn. Magn. Mater. 382 (2015) 335–341, https://doi.org/10.1016/j.jmmm.2015.01.085.

[11] T. Maeda, T. Kai, A. Kikitsu, T. Nagase, J.-i. Akiyama, Reduction of ordering temperature of an FePt-ordered alloy by addition of Cu, Appl. Phys. Lett. 80 (12) (2002) 2147–2149, https://doi.org/10.1063/1.1463213.

[12] G.L. Katona, N.Y. Safonova, F. Ganss, D. Mitin, I.A. Vladymyrskyi, S.I. Sidorenko, I.N. Makogon, G. Beddies, M. Albrecht, D.L. Beke, Diffusion and solid state reactions in Fe/Ag/Pt and FePt/Ag thin-film systems, J. Phys. D, Appl. Phys. 48 (17) (2015) 175001, https://doi.org/10.1088/0022-3727/48/17/175001.

[13] I.A. Vladymyrskyi, A.E. Gafarov, A.P. Burmak, S.I. Sidorenko, G.L. Katona, N.Y. Safonova, F. Ganss, G. Beddies, M. Albrecht, Y.N. Makogon, D.L. Beke, Low-temperature formation of the FePt phase in the presence of an intermediate Au layer in Pt /Au /Fe thin films, J. Phys. D, Appl. Phys. 49 (3) (2016) 035003, https://doi.org/10.1088/0022-3727/49/3/035003.

[14] Y. Wang, M. Jiang, R. Wang, Z. Wen, H. Li, Y. Ren, G. Qin, Au composition dependent order-disorder transitions of Fe-Pt intermetallic compounds: experiments and thermodynamic analysis, Acta Mater. 235 (2022) 118058, https://doi.org/10.1016/j.actamat.2022.118058.

[15] S.M. Zharkov, E.T. Moiseenko, R.R. Altunin, $L1_0$ ordered phase formation at solid state reactions in Cu/Au and Fe/Pd thin films, J. Solid State Chem. 269 (2019) 36–42, https://doi.org/10.1016/j.jssc.2018.09.009.

[16] S. Bahamida, A. Fnidiki, M. Coïsson, G. Barrera, F. Celegato, E. Olivetti, P. Tiberto, A. Laggoun, M. Boudissa, Effect of the A1 to $L1_0$ transformation on the structure and magnetic properties of polycrystalline $Fe_{56}Pd_{44}$ alloy thin films produced by thermal evaporation technique, Thin Solid Films 668 (2018) 9–13, https://doi.org/10.1016/j.tsf.2018.10.013.

[17] A. Kovács, K. Sato, Y. Hirotsu, High-resolution transmission electron microscopy analysis of L10 ordering process in Fe/Pd thin layers, J. Appl. Phys. 102 (12) (2007) 123512, https://doi.org/10.1063/1.2826632.

[18] M. Futamoto, M. Nakamura, M. Ohtake, N. Inaba, T. Shimotsu, Growth of $L1_0$-ordered crystal in FePt and FePd thin films on MgO(001) substrate, AIP Adv. 6 (8) (2016) 085302, https://doi.org/10.1063/1.4960554.

[19] H. Chang, F. Yuan, W. Chen, D. Wei, M. Lin, C. Wang, C. Shih, W. Chang, Magnetic property improvement of sputter-prepared FePd films on glass substrates with W underlayer, J. Alloys Compd. 622 (2015) 1013–1017, https://doi.org/10.1016/j.jallcom.2014.11.054.

[20] H.W. Chang, F.T. Yuan, W.C. Chen, D.H. Wei, M.C. Lin, C.C. Su, C.R. Wang, C.W. Shih, W.C. Chang, Y.D. Yao, Hard magnetic property improvement of sputter-prepared FePd films on glass substrates by underlayering with refractory Nb, Mo, and W elements, IEEE Trans. Magn. 51 (11) (2015) 1–4, https://doi.org/10.1109/TMAG.2015.2438896.

[21] B. Li, W. Liu, X. Zhao, S. Ma, W. Gong, J. Feng, F. Wang, Z. Zhang, Ordering temperature of $L1_0$-FePd film reduced by Ag underlayer, Mater. Lett. 100 (2013) 58–61, https://doi.org/10.1016/j.matlet.2013.02.102.

[22] P. Caro, A. Cebollada, F. Briones, M. Toney, Structure and chemical order in sputtered epitaxial FePd(001) alloys, J. Cryst. Growth 187 (3–4) (1998) 426–434, https://doi.org/10.1016/S0022-0248(98)00036-0.

[23] Y. Tokuoka, Y. Seto, T. Kato, S. Iwata, Effect of Ag addition to L1 FePt and L1 FePd films grown by molecular beam epitaxy, J. Appl. Phys. 115 (17) (2014) 17B716, https://doi.org/10.1063/1.4864251.

[24] M.N.I. Khan, N. Inami, H. Naganuma, Y. Ohdaira, M. Oogane, Y. Ando, Promotion of L 1_0 ordering of FePd films with amorphous CoFeB thin interlayer, J. Appl. Phys. 111 (7) (2012) 07C112, https://doi.org/10.1063/1.3673409.

[25] X. Wang, S. Krylyuk, D. Josell, D. Zhang, D. Lyu, J.-P. Wang, D.B. Gopman, Buffer layer engineering of L1 $_0$ FePd thin films with large perpendicular magnetic anisotropy, AIP Adv. 11 (2) (2021) 025106, https://doi.org/10.1063/5.0033287.

[26] M.N. Shamis, N.Y. Schmidt, T.I. Verbytska, P.V. Makushko, G. Beddies, M. Albrecht, Y.N. Makogon, L10 phase formation in FePd thin films induced by H2 during annealing, Appl. Nanosci. 12 (4) (2022) 1227–1233, https://doi.org/10.1007/s13204-021-01809-4.

[27] A. Götze, S.C. Stevenson, T.C. Hansen, H. Kohlmann, Hydrogen-induced order–disorder effects in FePd3, Crystals 12 (12) (2022) 1704, https://doi.org/10.3390/cryst12121704.

[28] L. Levchuk, R. Shkarban, I. Kotenko, K. Graivoronska, O. Fesenko, I. Lukianenko, T. Verbytska, I. Makogon, M. Barabash, Changes in Raman spectra upon formation of ordered $l1_0$ FePd phase during annealing in vacuum and in hydrogen atmosphere, Thin Solid Films 789 (2024) 140200, https://doi.org/10.1016/j.tsf.2024.140200.

[29] H. Naganuma, K. Sato, Y. Hirotsu, Perpendicular magnetic anisotropy of epitaxially grown L1-FePdCu nanoparticles with preferential c-axis orientation, J. Appl. Phys. 100 (7) (2006) 074914, https://doi.org/10.1063/1.2357420.

[30] A. Polit, D. Makarov, C. Brombacher, M. Krupinski, M. Perzanowski, Y. Zabila, M. Albrecht, M. Marszałek, Structural and magnetic properties of Cu-alloyed FePd films, J. Magn. Magn. Mater. 381 (2015) 316–321, https://doi.org/10.1016/j.jmmm.2015.01.017.

[31] V. Myagkov, O. Bayukov, Y. Mikhlin, V. Zhigalov, L. Bykova, G. Bondarenko, Long-range chemical interactions in solid-state reactions: effect of an inert Ag interlayer on the formation of L1 $_0$ -FePd in epitaxial Pd(0 0 1)/Ag(0 0 1)/Fe(0 0 1) and Fe(0 0 1)/Ag(0 0 1)/Pd(0 0 1) trilayers, Philos. Mag. 94 (23) (2014) 2595–2622, https://doi.org/10.1080/14786435.2014.926037.

[32] M. Perzanowski, Y. Zabila, M. Krupinski, A. Zarzycki, A. Polit, M. Marszalek, Chemical order and crystallographic texture of FePd: Cu thin alloy films, J. Appl. Phys. 111 (7) (2012) 074301, https://doi.org/10.1063/1.3699061.

[33] M. Perzanowski, M. Krupinski, A. Zarzycki, Y. Zabila, M. Marszalek, Structural ordering of laser-processed FePdCu thin alloy films, J. Alloys Compd. 646 (2015) 773–779, https://doi.org/10.1016/j.jallcom.2015.05.190.

[34] Y. Zhang, G. Cheng, X. Xu, L. Li, Effect of change in thickness of Ag toplayer on the structure and magnetic properties of FePd films grown on glass substrate, Journal of Wuhan University of Technology-Mater. Sci. Ed. 33 (5) (2018) 1082–1085, https://doi.org/10.1007/s11595-018-1938-1.

[35] S. Gulyás, G. Katona, Structural and phase transformations in Fe-Pd-Ag layered thin films below 500 °C, submitted for publication.

[36] H. Mehrer (Ed.), Diffusion in Solid Metals and Alloys, Landolt-Börnstein, New Series, vol. III/26, Springer, Berlin, 1990.

[37] F. Hartung, G. Schmitz, Interdiffusion and reaction of metals: the influence and relaxation of mismatch-induced stress, Phys. Rev. B 64 (24) (2001) 245418, https://doi.org/10.1103/PhysRevB.64.245418.

[38] A. Tynkova, G.L. Katona, G.A. Langer, S.I. Sidorenko, S.M. Voloshko, D.L. Beke, Formation of Cu_x Au_{1-x} phases by cold homogenization of Au/Cu nanocrystalline thin films, Beilstein J. Nanotechnol. 5 (2014) 1491–1500, https://doi.org/10.3762/bjnano.5.162.
[39] J. Chakraborty, U. Welzel, E.J. Mittemeijer, Interdiffusion, phase formation, and stress development in Cu–Pd thin-film diffusion couples: interface thermodynamics and mechanisms, J. Appl. Phys. 103 (11) (2008) 113512, https://doi.org/10.1063/1.2938079.
[40] F. Den Broeder, Interface reaction and a special form of grain boundary diffusion in the Cr-W system, Acta Metall. 20 (3) (1972) 319–332, https://doi.org/10.1016/0001-6160(72)90024-7.
[41] D. Beke, G. Langer, G. Molnár, G. Erdélyi, G. Katona, A. Lakatos, K. Vad, Kinetic pathways of diffusion and solid-state reactions in nanostructured thin films, Philos. Mag. 93 (16) (2013) 1960–1970, https://doi.org/10.1080/14786435.2012.732712.
[42] R. Balluffi, J. Cahn, Mechanism for diffusion induced grain boundary migration, Acta Metall. 29 (3) (1981) 493–500, https://doi.org/10.1016/0001-6160(81)90073-0.
[43] D. Beke, Y. Kaganovskii, G. Katona, Interdiffusion along grain boundaries – Diffusion induced grain boundary migration, low temperature homogenization and reactions in nanostructured thin films, Prog. Mater. Sci. 98 (2018) 625–674, https://doi.org/10.1016/j.pmatsci.2018.07.001.
[44] D. Yoon, Theories and observations of chemically induced interface migration, Int. Mater. Rev. 40 (4) (1995) 149–179, https://doi.org/10.1179/imr.1995.40.4.149.
[45] E. Rabkin, C. Ma, W. Gust, Diffusion-Induced Grain Boundary Phenomena in Metals and Oxide Ceramics, Materials Science Monographs, vol. 81, Elsevier, 1995, pp. 353–369.
[46] G. Schmitz, D. Baither, M. Kasprzak, T. Kim, B. Kruse, The hidden link between diffusion-induced recrystallization and ideal strength of metals, Scr. Mater. 63 (5) (2010) 484–487, https://doi.org/10.1016/j.scriptamat.2010.05.011.
[47] C. Feng, Q. Zhan, B. Li, J. Teng, M. Li, Y. Jiang, G. Yu, Magnetic properties and microstructure of FePt/Au multilayers with high perpendicular magnetocrystalline anisotropy, Appl. Phys. Lett. 93 (15) (2008) 152513, https://doi.org/10.1063/1.3001801.
[48] Y.-N. Hsu, S. Jeong, D.E. Laughlin, D.N. Lambeth, Effects of Ag underlayers on the microstructure and magnetic properties of epitaxial FePt thin films, J. Appl. Phys. 89 (11) (2001) 7068–7070, https://doi.org/10.1063/1.1360683.
[49] C. Feng, B.-H. Li, Y. Liu, J. Teng, M.-H. Li, Y. Jiang, G.-H. Yu, Improvement of magnetic property of L1-FePt film by FePt/Au multilayer structure, J. Appl. Phys. 103 (2) (2008) 023916, https://doi.org/10.1063/1.2828148.